BACHELOR

Recent advances and opportunities for MoS2 as charge extraction layer in Perovskite solar cells

Jansen, Jarvi W.P.

Award date:
2017

Link to publication

Technische Universiteit
Eindhoven
University of Technology

Department of Applied Physics
Plasma & Materials Processing

Recent Advances and Opportunities for MoS$_2$ as Charge Extraction Layer in Perovskite Solar Cells

J.W.P. Jansen

June 23, 2017

Supervisors:

MSc D. Koushik

Dr. M. Creatore

1. Abstract

Perovskite solar cells (PSCs) have emerged as one of the most promising photovoltaic technologies. However, the instability of perovskite is curbing its successful commercialization. Also, the now used organic charge transport layers in the device stack add to the instability of these perovskite devices. Hence, there is an urge towards replacing these organic charge transport layers with inorganic layers. MoS_2 has been a promising material because of its chemical inertness, good charge mobility (up to 470 $cm^2V^{-1}s^{-1}$ for electrons and 480 $cm^2V^{-1}s^{-1}$ for holes) and an appropriate valence band edge (5.2eV, close to the valence band of perovskite). This report is divided into two section. The first section describes the recent progress that have been made in implementing MoS_2 in PSCs. Thereafter, in the second section, the results employing atomic layer deposition (ALD) amorphous MoS_2 as hole transport layer in Cs-containing triple cation PSCs are presented. Being an ALD process, the deposited MoS_2 layers are ought to be more conformal and homogenous than solution and CVD processed MoS_2 layers. The Glass / ITO / ALD MoS_2 / triple cation perovskite / PCBM / ZnO / Al structured solar cells yielded a good fill factor of 66.2%, but a relatively low short-circuit current density of 7.8 mA cm^{-2} and open-circuit voltage of 527 mV compared to the reference solar cell. A power conversion efficiency (PCE) of 2.7% was achieved. The decreases in V_{OC} and J_{SC} are attributed to different grown perovskite crystals on the MoS_2, due to perovskite's poor wettability, which results in recombination at the perovskite/MoS_2 interface. If this recombination can be reduced, for example by pre-treatments, ALD MoS_2 as HTL presents a promising alternative towards replacing the organic HTLs employed in conventional PSCs, and hence towards gaining overall stability in the devices.

Contents

2. Introduction

Perovskite is emerging as the most promising material for solar cells. The material was first demonstrated in a solar cell in 2009 delivering an efficiency below 4%. [1] Within a short span of around 7 years, the perovskite based technology has already witnessed an efficiency of over 22%, approaching towards the efficiency of the c-Si global photovoltaic market leading technology. [2] [3] [4] Perovskite is also very cheap to produce and easy to manufacture. [5] However, a bottleneck towards commercializing perovskite solar cells is the instability of the intrinsic perovskite material against oxygen and moisture. A lot of research has been done to improve the stability of the intrinsic perovskite layer and the associated solar cells. The conventional hole transport layers (HTLs) employed in PSCs are organic. However, organic HTLs are susceptible towards degradation themselves. Of course, this is bad for the efficiency of the cells, so this demands investigation to find a better materials as hole transport layer in PSCs. MoS_2 has promising properties, like good charge carrier mobility and an appropriate valence band edge, to be applicable in PSCs. In this report, a literature overview of the recent advances on the application of crystalline MoS_2 in PSCs is presented. Thereafter, the results obtained via the implementation of amorphous MoS_2 (deposited via atomic layer deposition) as HTL in perovskite solar cells are presented. Finally, the opportunities to further enhance the performance of the fabricated ALD of MoS_2 based PSCs are discussed.

3. Perovskite

3.1 General structure

Perovskite is classified as a material that has the same type of crystal structure as calcium titanium oxide ($CaTiO_3$). [6] This general crystal structure is shown in figure 1.

The general class of Perovskite structure has the formula ABX_3, where 'A' and 'B' are often called the 'A-cation' and 'B-cation' respectively because these positions in the crystal structure hold the positive ions, and 'X' is called 'X-anion' because these positions hold negative ions. The crystal structure can be understood by starting with a face centered cubic (FCC) lattice filled with X-anions. Next, two adjacent atoms of the six face centered atoms X-anions are replaced by A-cations. Finally, four B-cations are placed in the intervening space in the crystal between two X-anions. This process is shown graphically in figure 2.
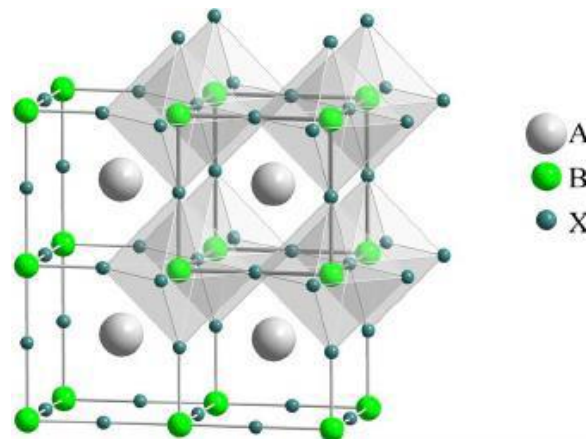

Figure 1: Illustration of the general crystal structure of perovskite.
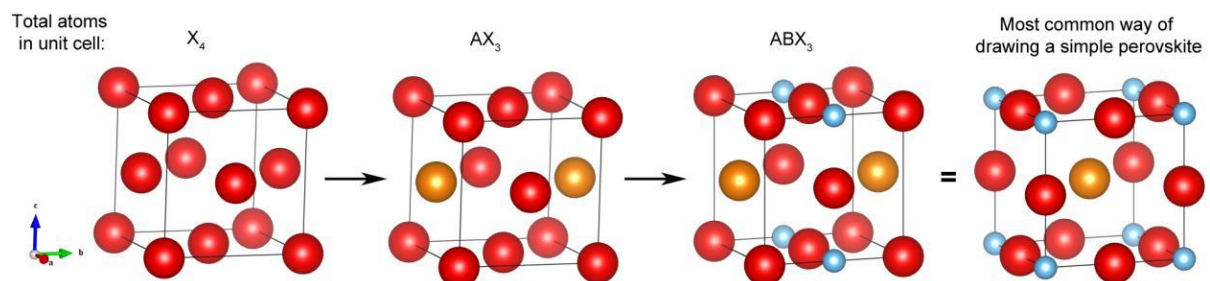

Figure 2: Visualisation of the process involved obtaining the unit cell of the perovskite structure. The red atoms represent the 'X-anion', the orange atoms represent 'A-cation' and the blue atoms represent 'B-cations'

3.2 Lead halide perovskite-based solar cells

The halogen group of the periodic table consists of the following five elements: Fluorine(F), Chlorine (Cl), Bromine (Br), Iodine (I) and Astatine(At). A halide is a binary compound formed by the combination of a halogen and a less negative element. Lead halide perovskites are perovskite structured compounds, where the lead ions (Pb^{2+}) are located at the A-cation site. The most investigated lead halide, with potential in solar cells, contain methylammonium ($CH_3NH_3^+$) at the B-cation.

For solar cells, methylammonium lead iodide ($CH_3NH_3PbI_3$) attracted attention in 2009. Research revealed that perovskite organo-lead mixed halide compounds exhibit excellent opto-electronic properties, also when deposited as thin films. This class of materials has a high absorption coefficient (>104 cm^{-1} above the band gap), long carrier diffusion length for both electrons and holes (in the range of 100–1000 nm), low non-radiative recombination rate and low excitonic binding energy (2–30 meV at room temperature). [7] The extreme rise of the power conversion efficiency of the perovskite-based devices is remarkable. Figure 3 demonstrates the power conversion efficiencies of the perovskite-based devices over recent years, in comparison to emergent photovoltaic research technology, and also traditional thin-film photovoltaics. In a few years, perovskite solar cells have managed to achieve power conversion efficiencies above 22%. The extreme rise in perovskite solar cell efficiency brings a lot of potential, also since these materials are cheap to produce and simple to manufacture. [8]
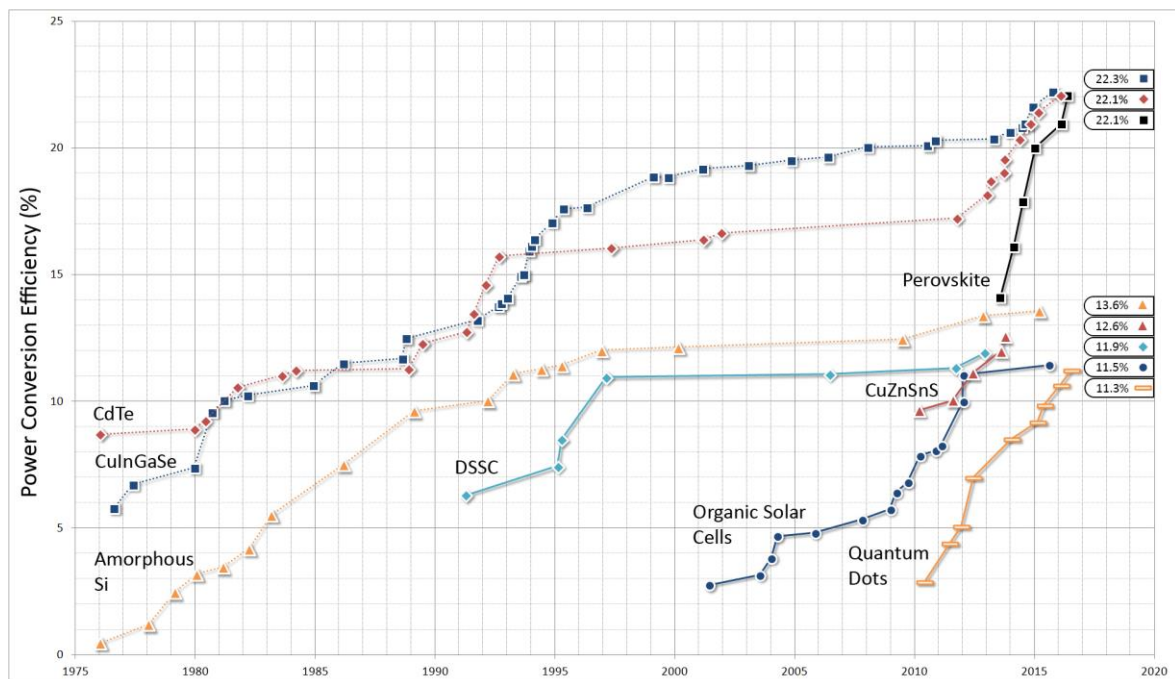

Figure 3: Power conversion efficiencies (%) over years for different photovoltaics.

There are different stacking configurations for perovskite solar cells. The four main structures are shown in figure 4. The mesoscopic n-i-p structure is the most popular structure reported in the literature. [9] The structure consists of a TCO cathode, a 50-70 nm thick compact ETM (typically TiO_2), a 150-300 nm thick mesoporous metal oxide (mp-TiO_2) that is filled with perovskites, followed by an up to 300 nm perovskite capping layer, a 150-200 nm thick layer of spiro-OMeTAD (hole conductor) and a 50-100 nm metal anode (Au or Ag). In this structure, the mesoscopic layer is thought to enhance charge collection by decreasing the carrier transport distance, preventing direct current leakage between the two selective contacts and increasing photon absorption due to light scattering. [10] First, thick (>500 nm) porous layers were used to efficiently absorb the incident light. Surprisingly, thinning the mesoporous layer to 150-200 nm improved the device efficiency due to enhanced crystallinity in the perovskite absorber.

The planar n-i-p structure doesn't have a mesoporous layer. The mesoporous layer seems critical for high-efficiency perovskite devices because hole extraction is significantly more efficient. Without the mesoporous layer, still an efficiency of 19.3% is achieved, but the state-of-the-are n-i-p devices usually include a thin (around 150 nm) mesoporous buffer layer filled and capped with the perovskite. [11]

When the deposition order is changed and the HTM layer is deposited first, the device is fabricated in the p-i-n configuration. The efficiency of the planar p-i-n device has improved significantly due to better material preparation methods, resulting in a best efficiency of 18.9%. The best mesoscopic p-i-n device with a nanostructured NiO film showed an efficiency of 17.3%.
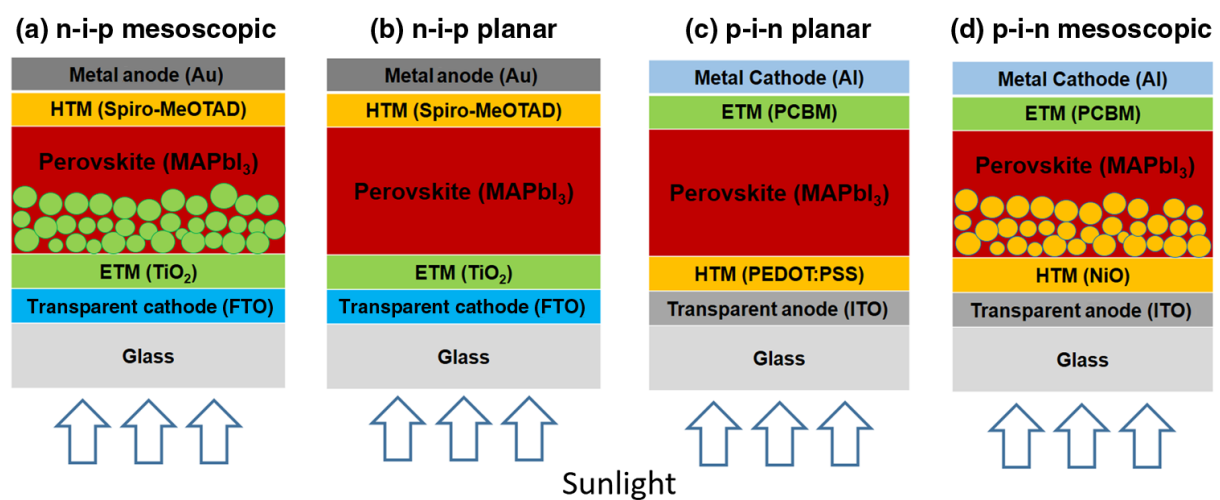

Figure 4: Schematic diagrams of perovskite solar cells in the (a) n-i-p mesoscopic, (b) n-i-p planar, (c) p-i-n planar, and (d) p-i-n mesoscopic structures.

3.3 Instability of perovskite

The major issue with perovskite solar cells is the instability of the intrinsic perovskite material. Niu et al. found four key factors causing degradation of the perovskite film: oxygen and moisture, UV light, solution processing and thermal effects. [12] Illumination with UV light can cause degradation in perovskite solar cells. Reports shown that by UV-illumination, the TiO_2 in perovskite solar cells causes degradation. [13] At the interface between the TiO_2 layer and the perovskite, TiO_2 can extract electrons from I^- and produce I_2. This will lead to breakdown of the perovskite crystal. [14] Exposure to high temperatures also causes degradation of the perovskite layer. Understanding this is really important, as the perovskite layers requires an annealing step and of course solar cells will be confronted with high temperatures of the sun. Multiple reports have monitored the thermal stability of the perovskite under vacuum conditions, all concluding that annealing at high temperatures ($> 150 °C$) causes deposition to PbI_2. So overheating could lead to serious decomposition of perovskite and lead to poor device performance. [14] However, to be able to commercialize perovskite solar cells, the degradation of perovskite by influence of moisture and oxygen is the most important problem to overcome. Multiple reports have suggested that water is the catalyst required for the irreversible degradation of perovskite. The highly hydrophilic properties of perovskite can cause the materials to easily absorb moisture from the surrounding environment and induce the formation of hydrate products. [15] The degradation of perovskite is a problem for the lifetime of photovoltaic cells. Another problem caused by the degradation process with water are the by-products. One of the by-products is PbI_2, which could cause eco-toxicological problems. [16] Knowing this, it is obvious that the perovskite layer should get protected from the moisture. Right now, mostly organic HTLs are used in perovskite solar cells. Organic HTLs poorly protect the perovskite layer from the moisture and oxygen, and are susceptible for degradation themselves. [7] Now more and more research is done towards the use of inorganic materials as HTL in PSCs, cause inorganic materials can protect the perovskite layer from moisture and oxygen.

4. MoS$_2$

4.1 MoS$_2$ structure and properties

MoS$_2$ is a transition metal dichalcogenides (TMD), exhibiting similar layered structure as graphene. A single layer of MoS$_2$ is composed of a sheet of molybdenum (Mo) sandwiched by sulphur (S) atoms, arranged in a trigonal prismatic coordination, where each sulphur atom is bonded to 3 Mo atoms. A monolayer of MoS$_2$ is shown in figure 5. Bulk MoS2 is formed by several tri-layer basic structures held together by van der Waals forces. [17]

A very interesting property of MoS$_2$ is that the thickness of a MoS$_2$ layer influences its electronic and optical properties. Dashora et al. investigated this and computed the electronic and optical properties of MoS$_2$ thin film for different thicknesses (1-14 layers of MoS$_2$). [18] A monolayer of MoS2 possess a direct band gap of 1.8 eV whereas multi-layered MoS2 has a band gap of 1.2 eV. The surface energies and work functions are computed as a function of the film thickness and shown in table 1. The oscillations in surface energy and work function below 8 layers predict the presence of quantum size effect at the lower thicknesses. Figure 6 shows the energy bands of bulk MoS$_2$ along with the MoS$_2$ (0 0 0 1) thin films with different layers (1-14 L).
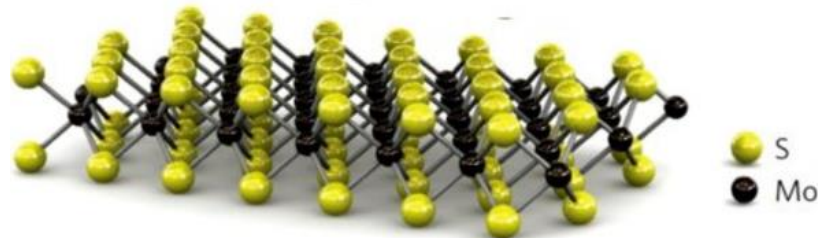

Figure 5: Image of monolayer MoS$_2$.

N (L)	Thickness (Å)	Surface energies E_S (eV)	Work function W (eV)
2	12.26	0.06	5.55
4	24.52	0.07	5.42
6	36.78	0.08	5.35
8	49.04	0.06	5.35
10	61.30	0.06	5.35
12	73.56	0.05	5.35
14	85.82	0.05	5.35

Table 1: Surface energies (ES) and work functions (W) for MoS2 (0 0 0 1). N stands for number of layers.

To check the applicability of MoS_2 thin films in solar cells, the total absorption from 0 to 5 eV is calculated. These values of total absorption (TA) for the perpendicular and parallel components are given in Table 2. Monolayer of MoS_2 shows small values of absorption coefficients and the total absorption increases with an increase in film thickness. For 14 layers it almost reaches the bulk value. It is concluded that 8 layers of MoS_2 reproduce very well the absorption and dielectric features of bulk material.

MoS_2 serves as an attractive candidate as hole transport layer (p-type semiconductor from energy band diagram) cause of its chemically inertness, good charges mobility (up to 470 $cm^2V^{-1}s^{-1}$ for electrons and 480 $cm^2V^{-1}s^{-1}$ for holes) and an appropriate valence band edge (5.2eV, close to the valence band of perovskite). [19] [20] Also the variation in band gap energy (1.29 eV for multilayer MoS_2 and 1.9 eV for monolayer MoS_2) and the change of band gap by varying the layer thickness (monolayer MoS_2 has a direct bandgap and multilayer MoS_2 has an indirect bandgap) make the few-layer MoS_2 film extremely beneficial as a photovoltaic material for absorbing solar energy. [21] Furthermore, the good atmosphere stability (MoS_2 is an inorganic hydrophobic material) of MoS_2 and its transparency are properties that gave MoS_2 potential as hole transport layer in solar cells.
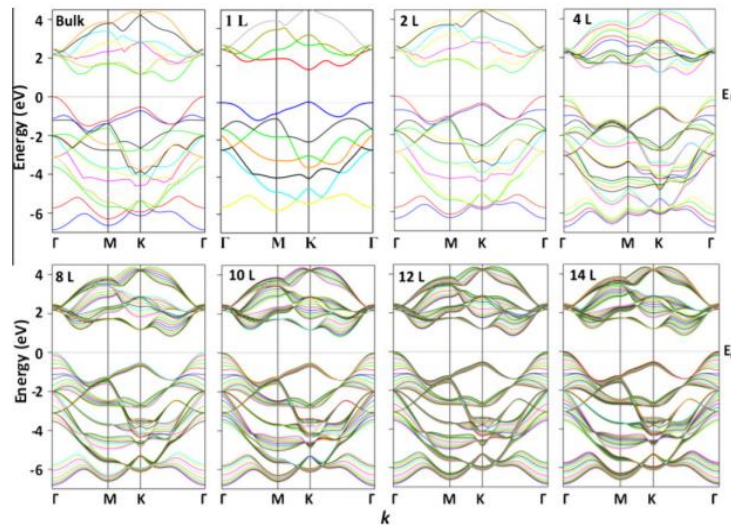

Figure 6: Energy bands for bulk MoS2 and thin films (for 1 L to 14 L) of MoS2 along (0 0 0 1) direction. L stands for layer.

N	Total absorption (0–5 eV) x 10^4 eV/cm		Dielectric constant	
	$\alpha_\perp$	$\alpha_\parallel$	$\varepsilon_{1\perp}(0)$	$\varepsilon_{1\parallel}(0)$
Bulk	277.28	123.41	15.76	10.09
1 L	86.42	18.63	2.99	2.02
2 L	183.26	66.11	7.79	4.91
4 L	216.35	88.45	10.23	6.61
6 L	231.56	98.18	11.49	7.45
8 L	240.69	103.27	12.27	7.95
10 L	245.96	106.36	12.76	8.28
12 L	249.24	109.45	13.08	8.55
14 L	253.31	111.23	13.41	8.74

Table 2: Total absorption coefficients (in the range 0-5eV) and dielectric constants for bulk and different layers of MoS2 (0 0 01) thin films.

4.2 Atomic Layer Deposition (ALD) of MoS_2

There are different ways to synthesize MoS_2. The MoS_2 films used in this report are grown by plasma enhanced ALD. Atomic layer deposition (ALD) is a vapour phase deposition technique that holds promises to deposit ultra-thin films with precise thickness control and excellent repeatability. A typical ALD process consists of alternating repetition of half-cycles of precursor dose and co-reactant exposure. [22]. A typical ALD cycle is shown schematically in figure 7. The precursor is typically an metal-organic coordination compound. A self-limiting growth is obtained as result of occupation of all the available surface sites. For sufficient exposure of precursor and the co-reactant, a saturated growth is obtained, whereas an insufficient exposure results in incomplete saturation. The purge steps after dosing the precursor and exposing the co-reactant are very important. The excess precursor or co-reactant needs to get removed to avoid reactions between precursor and co-reactant molecules, as this could lead to undesired chemical vapour deposition reactions (CVD) [23]. The thickness of the atomic layer can be controlled by the numbers of repetitions of the ALD cycle [24]. As explained before (4.1), the properties of MoS_2 do change a lot by varying the thickness of the MoS_2 layer. Because with ALD the thickness can be controlled, ALD is a very useful technique for the synthesize of MoS_2.
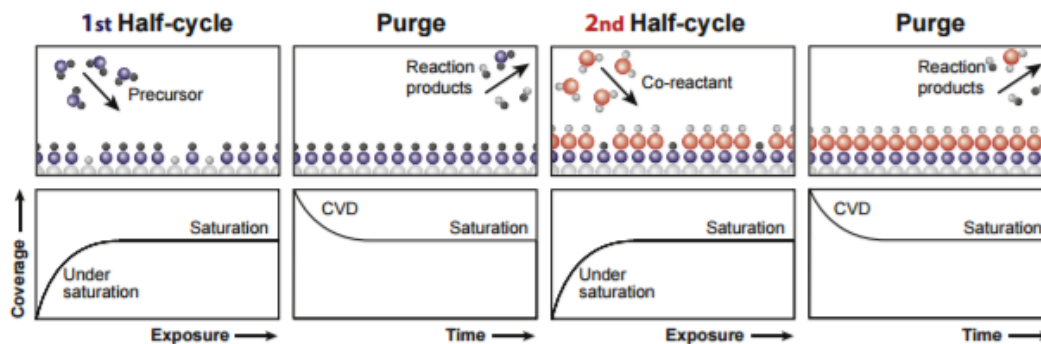

Figure 7: A schematic representation of the various steps in an ALD cycle consisting of two half reactions. The lower panels show the resulting coverage, or growth per cycle, as a function of exposure or time for that particular step.

5. MoS$_2$ in perovskite-based solar cells: literature overview

Electron and hole transport layers are very important in perovskite solar cells (PSCs) in a planar p-i-n junction structure. Poly(3,4-ethylenedioxythiophene): poly(- styrenesulfonate) (PEDOT:PSS) is conventionally used as the hole transporting layer in the PSCs. PEDOT:PSS is one of the best p-type semiconductors, however it is not suitable for practical applications due to fast degradation of organic layers and organolead halide perovskites layer occurs. Kim et al. used crystalline MoS$_2$, WS$_2$ and graphene oxide (GO) instead of PEDOT:PSS as hole extraction layer (HEL) in organolead halide perovskite solar cells. [25] The MoS$_2$ layer was synthesized by chemical vapor deposition (CVD) method. It was shown that the perovskite structure was well-formed on the MoS$_2$ layer.

For the synthesis of MoS2, a SiO2 (300 nm)/Si wafer was used as insulating substrate. MoS$_2$ thin layers were prepared by CVD using a uniformly spin-coated (NH$_4$)MoS$_4$ and (NH$_4$)WS$_4$ precursor solutions. The thickness of the MoS$_2$ was approximately 2 nm. CH$_3$NH$_3$PbI$_{3-x}$CL$_x$ was used as the absorber layer for the solar cell fabrication.

After the MoS$_2$ was synthesized, poly [methyl methacrylate] (PMMA) is spin-coated on the MoS2 layer. Then, the substrate was immersed into a hydrogen fluoride and aluminium fluoride (1:1) bath at room temperature for 1 h to etch away the SiO$_2$ layers. Subsequently, the remaining MoS$_2$ layer was carefully dipped into a DI water bath 7-9 times to remove any residual etchant. The MoS$_2$ sheet was then transferred onto an indium tin oxide (ITO) substrate. Finally, the PMMA membrane was removed by an acetone bath at 50 °C for 30 min after which the PMMA/MoS$_2$ layer had completely adhered to the target substrate.
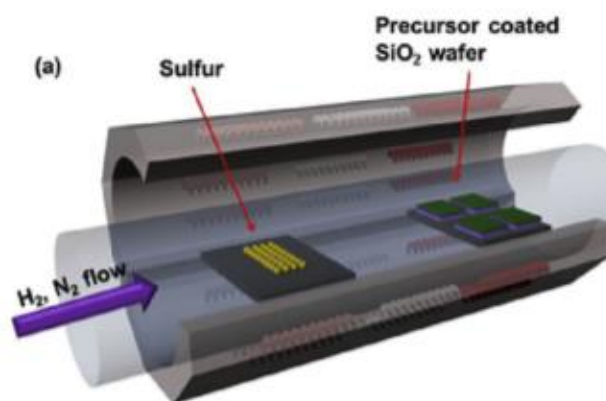

Figure 8: (a) Schematic of chemical vapor deposition (CVD) synthesis for MoS2 layer.

For fabricating the PSCs, an ITO glass was used as the substrate. Its surface was cleaned and the samples were treated with UV/ozone (UVO) for 15 minutes. After the treatment of the substrate, the MoS_2 layer was formed at the active area and loaded into a N_2-filled glove-box. A (4:1:1 M ratio) solution of perovskite precursor in DMF was spin-coated at 4000 rpm for 30 s to prepare the perovskite films. The substrates were heated at 100 °C under dry conditions for 60 min. The PCBM solution was also spin-coated (700 rpm, 15 , 40 nm) on top of the $CH_3NH_3PbI_{3-x}CL_x$ active layer. The BCP layer was used as hole transport layer.

Field-emission scanning electron microscopy (FE-SEM) images were taken to measure the thickness of the layers and the surface state. The X-ray diffraction (XRD) pattern transmission electron microscope (TEM) images were obtained to measure the structures and the sizes of the perovskite materials. Contact-mode atomic force microscopy (AFM) was used to measure the surface root-mean-square (RMS) roughness. Figure 10a shows the top view of the MoS_2 FE-SEM image. The surface of MoS_2 is smooth. The energy dispersive spectra confirms that the synthesized film is MoS_2. Figure 10b shows the TEM image of MoS_2. The periodic atomic arrangements of the MoS_2 are shown in the inset. The hexagonal structure indicated that single-crystalline MoS_2 layers were synthesized. In the TEM images in other areas, a non-periodic atomic arrangement were found, indicating the presence of polycrystalline areas in the synthesized MoS_2 The AFM image of MoS_2 is shown in figure 10c. The RMS roughness value was measured to be 1.391 nm. This roughness value is low enough to spin-coat the perovskite layer on the hole extraction layer.
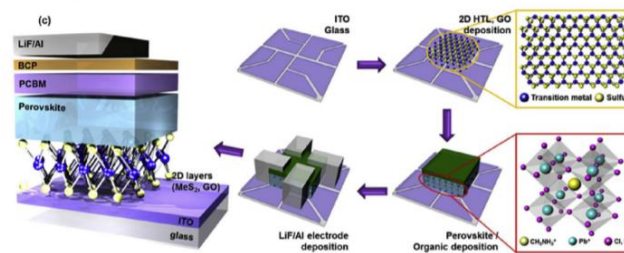

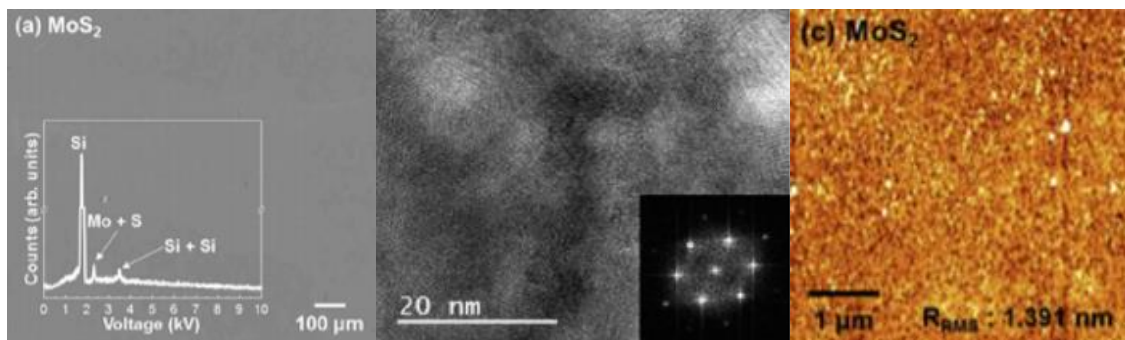Figure 9: Schematic of PSC fabrication procedure and device structure.

Figure 10: a) Top view of FE-SEM) images of synthesized MoS2. The scale bar is 100 μm. b) The high resolution TEM images of synthesized MoS2. The periodic atomic arrangement of the MoS2 film is shown in the inset. c) AFM image of MoS2.

Kim et al. also tested the perovskite layer to see its characteristics. The XRD measurement showed two intense peaks located at 14.1° and 28.3° and two weak peaks located at 43.2° and 58.8°. Several other peaks were showed, which suggest that the perovskite layer formed is $CH_3NH_3PbI_{3-x}CL_x$.

FE-SEM images of the perovskite layer were made and shown in figure 11. The film shows nearly uniform contrast and grain size across the entire field of view. According to the cross-sectional view of the FE-SEM image, the thickness of the $CH_3NH_3PbI_{3-x}CL_x$ is measured to be around 330 nm.

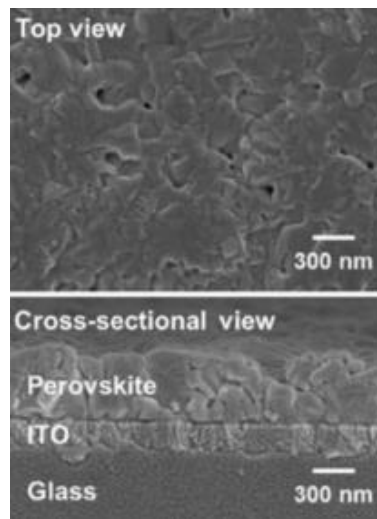*Figure 11: FE-SEM images of $CH_3NH_3PbI_{3-x}CL_x$ layer for top-view and cross-sectional view.*
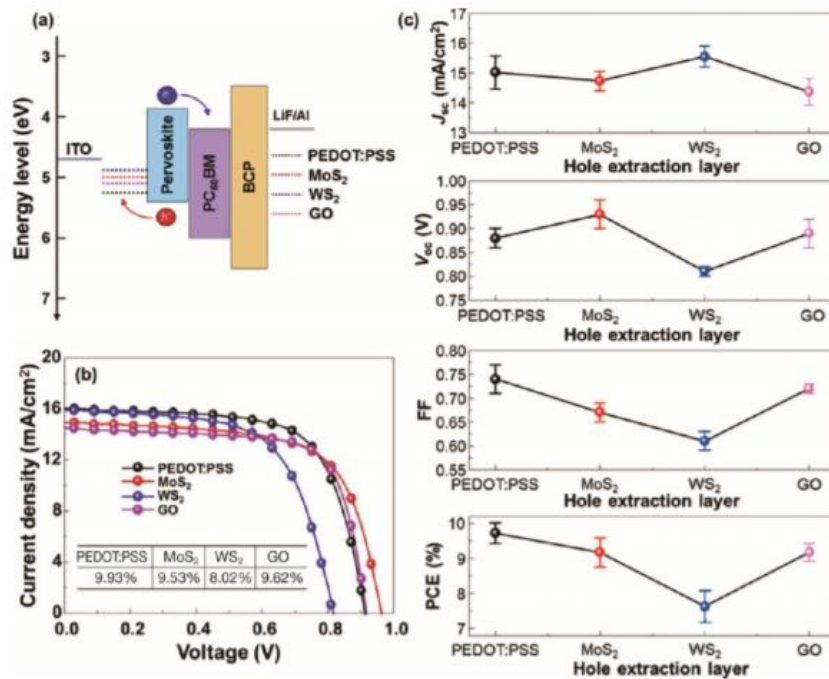

Figure 12: (a) Energy band diagram of fabricated PSCs. (b) Current density-voltage curves of each different HEL-based PSCs. The maximum efficiency of PEDOT:PSS, MoS2, WS2, and GO layers are 9.93%, 9.53%, 8.02%, and 9.62%, respectively. (c) The statistical analysis of device characteristics for different 5 batch fabrications (20 cells).

After testing the characteristics of the MoS_2 and the perovskite layer, the perovskite solar cell with different hole transport layers were tested. The fabricated perovskite solar cell was glass ITO/ 2 nm MoS_2/ $CH_3NH_3PbI_{3-x}CL_x$ / PCBM/BCP (HBL)/ LiF, Al structured. Figure 12 shows the energy band diagram, the current density-voltage curves and the device characteristics for the perovskite solar cells with different hole transport layer.

The energy band diagram suggests that the work function of MoS_2 is suitable for the HEL in the PSCs. The transmittance value of MoS_2 is greater than 90%, so that almost all the light can reach the perovskite active layer. The open-circuit voltage (V_{oc}), short-circuit current (J_{sc}), fill factor (FF) and the power conversion efficiency (PCE) of the MoS_2 based PSCs are 0.96V, 14.89 mA/cm^2, 0.67 and 9.53% respectively. Therefore is concluded that MoS_2 can be used as hole transport layer in perovskite solar cells.

Capasso et al. used MoS2 flakes as hole transport layer (HTL) in combination with spiro-OMeTAD to fabricate metal-organic perovskite solar cells. [17] MoS2 bulk crystals are exfoliated in 2-propanol and deposited on perovskite layers by spray coating on a hot-plate at 60 °C. Thick and un-exfoliated MoS_2 were removed. After the preparation of the MoS2 dispersion, optical absorbance spectroscopy was performed. The absorption spectrum showed two peaks at 612 and 675nm, which are signature of the characteristic A and B excitonic transitions of MoS2, respectively [26]. The TEM analysis in figure 13 shows the presence of exfoliated flakes with a lateral size in the order of 100-200nm. In the inset, the electron diffraction pattern shows the hexagonal crystalline structure characteristic of MoS2 flakes.
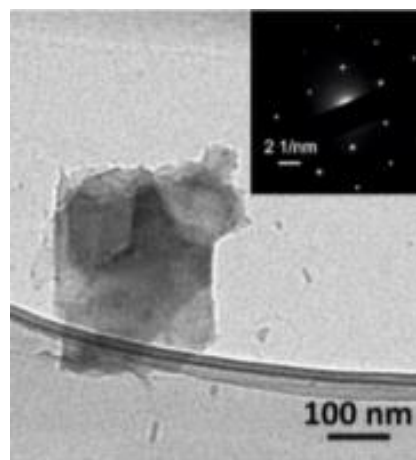

Figure 13: TEM image of exfoliated MoS2 flakes. Inset: electron diffraction pattern.

The glass/FTO/compact-TiO2/mesoporousTiO2/CH3NH3PbI3/spiro-OMeTAD/Au based solar cells were developed with MoS2 flakes instead of spiro-OMeTAD. After testing cells with spray-coated MoS_2, varying the thickness of the TiO_2 mesoporous layer in the 250-500nm range, the highest PCE was reached with a TiO_2 thickness of 250nm. Hereafter, the I/V characteristics of the MoS_2-based PSCs with 250nm of TiO_2 and the PSCs based on Spiro-OMeTAD were tested. The results are shown in figure 14 and table 3.

The solar cells with MoS_2 as HTL exhibited a PCE of 3.9%, compared with a PCE of 3.1% for spiroOMeTAD as HTL. The CH3NH3PbI3/MoS2/spiro-OMeTAD/Au based solar cell device exhibited a PCE of 13.09%. The MoS_2-based cells showed higher stability ($\Delta PCE/PCE$=-17%) than that of doped spiro-OMeTAD-based solar cells ($\Delta PCE/PCE$ =-45%), during an endurance test conducted on 800 h shelf life (see figure 15). Both types of solar cells, with, and without, MoS_2 as HTL, show a drastic decrease in PCE values from 400 to 800 h, from the degradation of the perovskite layer due to air exposure.
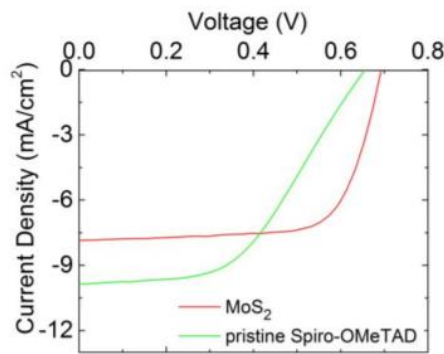

Figure 14: I/V characteristics of perovskite-based cells (with 250nm of mesoporous TiO2) with MoS2 flakes as HTL and with pristine Spiro-OMeTAD.

	V_{oc} (V)	J_{sc} (mA/cm^2)	FF	η
MoS$_2$	0.69	-7.75	72.2%	3.9%
Spiro-OMeTAD	0.66	-9.86	48.7%	3.1%

Table 3: I/V parameters of perovskite-based cells (with 250 nm of mesoporous TiO2) with MoS2 flakes as HTL and with pristine Spiro-OMeTAD.
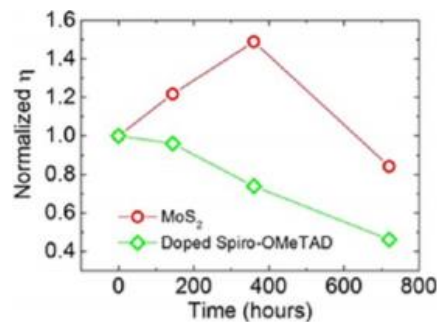

Figure 15: Endurance test on 800 h shelf life for glass/FTO/compact-TiO2/mesoporous-TiO2/CH3NH3PbI3/spiro-OMeTAD/Au based solar cells with MoS2 and doped Spiro-OMeTAD as a hole transport layer (HTL), showing higher stability for the MoS2-based solar cells

Capasso et al. demonstrated that in glass/FTO/compact-TiO2/mesoporous-TiO2/CH$_3$NH$_3$PbI$_3$/MoS$_2$/Spiro-OMeTAD/Au based solar cells, MoS2 flakes act both as a HTL from the perovskite to the Spiro-OMeTAD, and as a protective layer between perovskite and Au electrode. [20]

Solar cells with MoS$_2$ showed a PCE of 13.3% and higher stability compared with the reference solar cells without MoS$_2$. Also the use of MoS$_2$ was found to improve the shelf life of large-area perovskite-based solar cells.

Bulk MoS$_2$ was exfoliated in NMP (N-methyl-2-pyrrolidone) solvent, since it has a surface tension matching the surface energy of the exfoliated flakes, obtaining dispersions of MoS$_2$ flakes. The obtained dispersion was ultracentrifuged to remove thick and un-exfoliated MoS$_2$ flakes. After that, a solvent-exchange process is used to re-disperse the MoS$_2$ flakes in IPA (isopropyl alcohol). The NMP is detrimental for the perovskite layer so needs to get removed. This is done with a rotary evaporator and an ultracentrifuge. Hereafter the IPA solvent was evaporated at 60 °C to collect the MoS$_2$ powder. The flakes were dried in vacuum in 200 °C for 2 hours to further purify the material, which was then re-dispersed in 1 mL of IPA. Finally, the purified MoS$_2$ flakes in IPA are spin-coated onto the perovskite layer at 1700 rpm for 45 s and annealed for one minute at 70 °C.

Capasso et al. demonstrated that the solvent-exchange process does not affect the structure of the liquid-phase exfoliation MoS$_2$ flakes. The thickness of the exfoliated MoS$_2$ flakes is evaluated by atomic force microscopy (AFM) measurements. The flakes' thickness is in the 1-5 nm range, indicating the presence of few-layer MoS$_2$ flakes. Raman spectroscopy was performed on bulk MoS$_2$ as well as on the exfoliated flakes in NMP and IPA. The Raman spectra are shown in figure 16. The Raman spectra shows clear peaks which indicates a crystalline structure. The Raman spectra analysis demonstrates that the solvent-exchange process does not affect the structure of the liquid-phase exfoliation MoS$_2$ flakes.
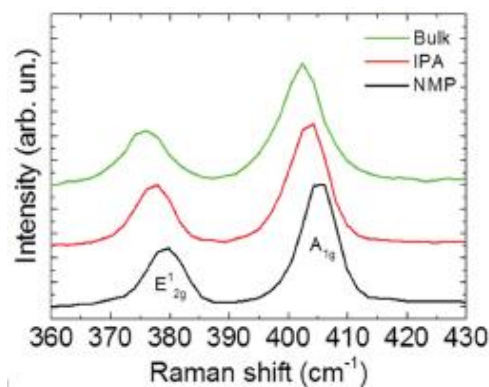

Figure 16: Raman spectra at 532 nm excitation wavelength of bulk and exfoliated MoS$_2$ cast on Si/SiO$_2$.

The MoS$_2$ flakes in IPA were spin-coated onto the perovskite layer to create the active buffer layer. Scanning electron microscopy (SEM) images were taken after the deposition to evaluate the surface coverage. By exploring all the parameters involved in the MoS$_2$ deposition process (spin coating time, speed, number of coating, post-annealing steps etc.), a planar layer of flakes that covers the perovskite crystals was formed (shown in figure 17 and 18). Although not all of the perovskite crystals were covered, these deposition parameters were chosen as a trade-off between uniform and planar deposition and minimal buffer layer thickness.
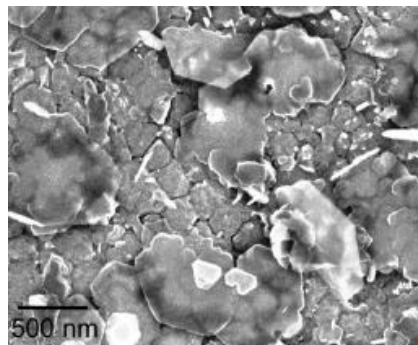

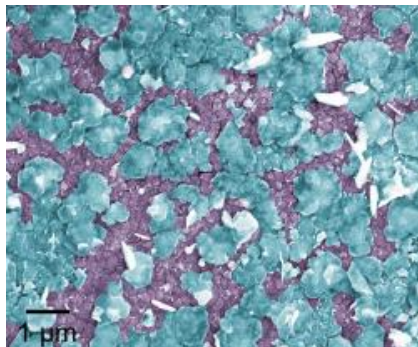*Figure 17: SEM image of MoS$_2$ flakes on top of the perovskite crystals.*

Figure 18: SEM image of the MoS$_2$ flakes spin-coated onto the perovskite layer (blue for MoS$_2$ flakes and purple for the underlying perovskite layer.

The efficiency of the MoS_2 layer as HTL depends on the alignment between the valence band maximum of MoS_2 and $MAPbI_3$. A small energy offset between the two bands results in an efficient hole collection at the Au electrode. [19] [27] The valence band maximum of the MoS_2 deposited on a Si substrate was measured to be -5.1 eV, close to that of $MAPbI_3$ (-5.4 eV).

To fully assess the performance of MoS_2 as active buffer layer, PSCs with glass/FTO/compact/TiO_2/mesoporous-TiO_2/$CH_3NH_3PbI_3$/MoS_2/Spiro-OMeTAD/Au structure were fabricated. The results of the *I/V* measurements under illumination are shown in figure 19. In comparison with the reference PSCs, the cells with MoS_2 buffer layer show an increase in J_{SC} (-21.5 vs. -18.8 mA cm^{-2}) and a decrease in V_{OC} (0.93 V vs. 1.01 V) and fill factor (66.7% vs. 74.6%). This results in an efficiency of 13.3% for the cells with MoS_2 (and 14.2% for the reference PSCs). The PSCs were measured again under illumination after 170 h, resulting in an efficiency of 13.5% (and 10.9% for reference PSCs). Also after 550 h were the PSCs measured. The graphs are shown in figure 20. The figure shown a significantly lower decrease in efficiency for the PSCs with MoS_2 (7% vs. 34% decrease in η). The improved stability of the MoS_2-based PSC with respect to the reference cell can be explained by the prevented iodine migration from the perovskite into the Spiro-OMeTAD cause of the provided surface passivation by the MoS_2 buffer layer. [28]
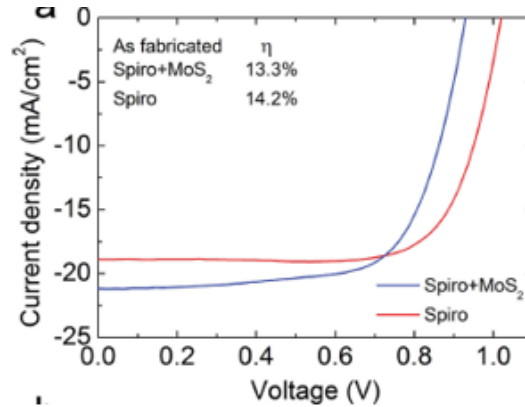

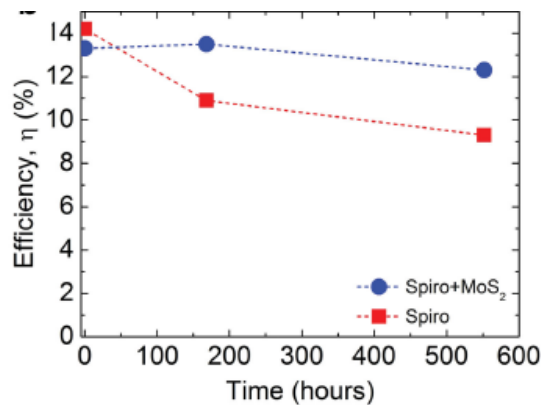*Figure 19: I/V curves of the PSCs measured after fabrication (0.1 cm² active area).*

Figure 20: Efficiency of PSCs with (blue) and without (red) MoS₂ over 550 h.

Also MoS$_2$-based PSCs with an active area of 1.05 cm^2 are fabricated to find out if the MoS$_2$-based PSCs also show good results for larger cell size. The *I/V* characteristics for large-area cells are shown in figure 21. The efficiency of the cell with MoS$_2$ now achieved around the same value as the reference cell (11.5% vs. 11.4%), confirming the results obtained for small-area cells. Furthermore the incident photon-to-electron conversion efficiency (IPCE) is measured for the two cells. The graphs of the two cells have the same shape, although the graph of the MoS$_2$-based cell shows an around 10% higher IPCE value in the 350-750 nm range. These IPCE trends are in agreement with the integrated current density values calculated from 300 to 850 nm. The graph is shown in figure 22.

Also the *I/V*-characteristics for perovskite solar cells with and without MoS$_2$ are measured to investigate the stability. The *I/V*-characteristics were measured after 7 and 23 days, by placing the devices in a desiccator having 30% relative humidity in dark conditions. Both *I/V*-characteristics are shown in figure 23. The PCE of perovskite solar cells having spiro+MoS$_2$ showed both times a higher stability, compared with the cells without MoS$_2$.
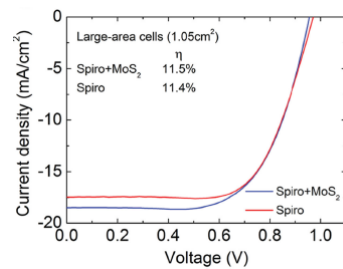

Figure 21: I / V curves of the large-area cells (1.05 cm^2 active area) with (blue curve) and without MoS$_2$ (red curve) measured under illumination.
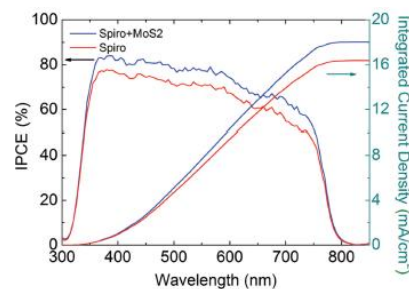

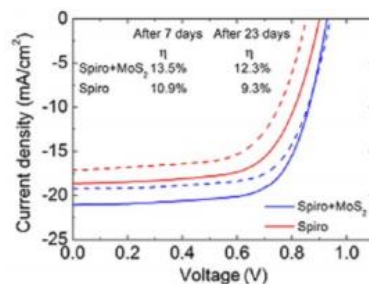*Figure 22: IPCE spectra and the integrated current densities of the two cells.*

Figure 23: I−V curves of the perovskite solar cells both Spiro-OMeTAD+MoS2, and spiro-OMeTAD alone, measured after aging for 7 and 23 days, where solar cell devices were stored in a desiccator.

6. Project goal

Cause perovskite is unstable, many materials are investigated to use as hole transport layer in PSCs to improve the stability and efficiency of the solar cells. Looking at the properties of MoS_2, it seems a very good material to use as hole transport layer in a perovskite solar cell. The goal of this project is to investigate the opportunities for MoS_2 as charge extraction layer in PSCs to improve the stability and efficiency.

7. Experimental setup

There are different methods to use MoS_2 in perovskite solar cells. Either the MoS_2 can be grown on perovskite (as reported by Kim et al.) perovskite can be deposited on MoS_2. There can also be difference in the structure of the MoS_2. In the most literature, the use of highly crystalline form of MoS_2 is reported. Here, we deposited the perovskite layer on amorphous MoS_2, which was synthesized by ALD at 150 °C. The MoS_2 films are grown by plasma enhanced atomic layer deposition (ALD). Argon is used as carrier gas. After the stabilization of the gas flow, the flow is diverted into the bubbler containing the metal precursor, thereby introducing the precursor into the reactor chamber (figure 24a) .The molybdenum metal precursor ($C_{12}H_{30}N_4Mo$) is contained in a stainless steel bubbler, held at a temperature of 50 °C. An exposure time of 6 seconds is found to be sufficiently enough to ensure that the half reaction is saturated. Thereafter, the chamber is purged with Argon in order to remove the reaction byproducts and un-reacted precursor from the chamber in order to suppress the CVD-type growth. The temperature of the walls and the stage is maintained at 150 °C. Subsequently, the plasma of diluted H_2S is ignited via inductively coupled rf source (ICP) operated at 13.56 MHz. The plasma consists of H_2S, H_2 and Argon (ratio 8:2:40) gas mixture. For the plasma, an exposure time of 20 seconds is entailed to ensure the saturation of surface reactions. This completes one ALD cycle for the synthesis of sub-monolayer MoS_2. The thickness of the MoS_2 layer can be controlled by changing the number of cycles.
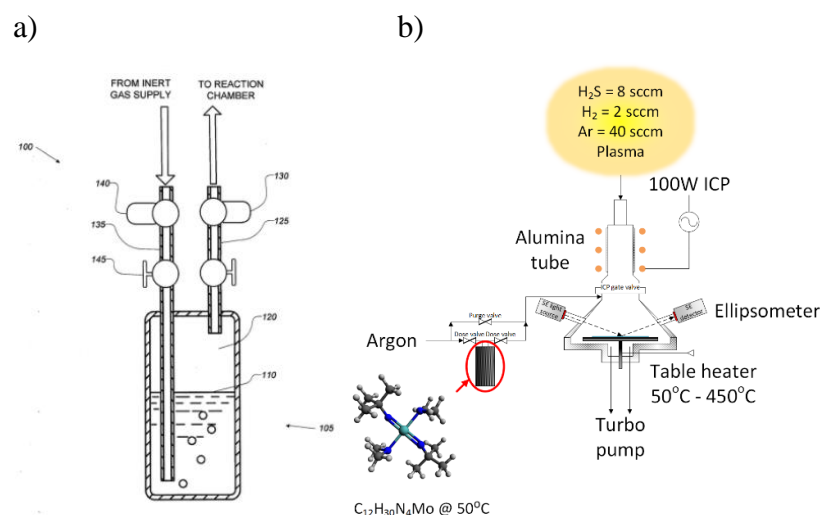

Figure 24: a) With the left pipe the precursor flows into the liquid, which results in bubbling. With the right pipe, a vapor of mixed precursor and argon goes to the reaction chamber. b) ALD recipe for MoS2 schematically

After the MoS$_2$ was synthesized, XRD and Raman measurements are done for MoS$_2$ films grown at different stage temperatures (T$_s$). The XRD spectra, shown in figure 25, illustrates increasing peak intensity with increasing temperature, signifying formation of crystalline MoS$_2$. Similarly the Raman spectra, shown in figure 26, shows increasing peak intensity for higher T$_s$. So from these results, it can be concluded that for 150 °C, amorphous MoS$_2$ is deposited, and for higher temperatures (>250 °C) nanocrystalline material is deposited. Also from the SEM measurment, shown in figure 27, the amorphous and nanocrystalline structure for different surface temperatures are clearly visible. The MoS$_2$ used in our solar cell is deposited at 150 °C.
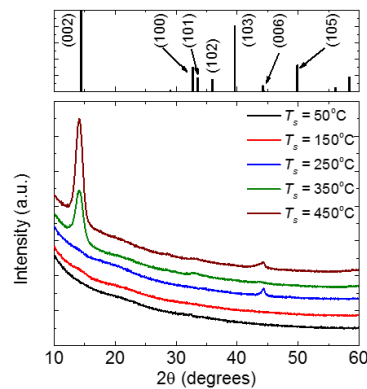

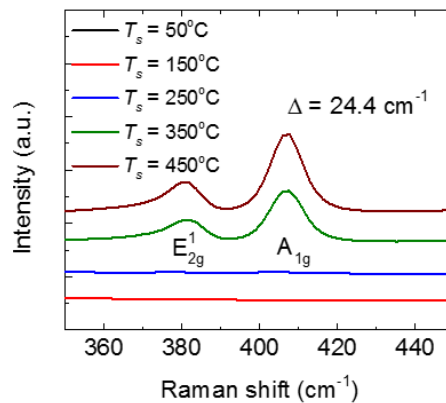*Figure 25: XRD spectra synthesized MoS$_2$ for different surface temperatures.*

Figure 26: Raman spectra synthesized MoS$_2$ for different surface temperatures.
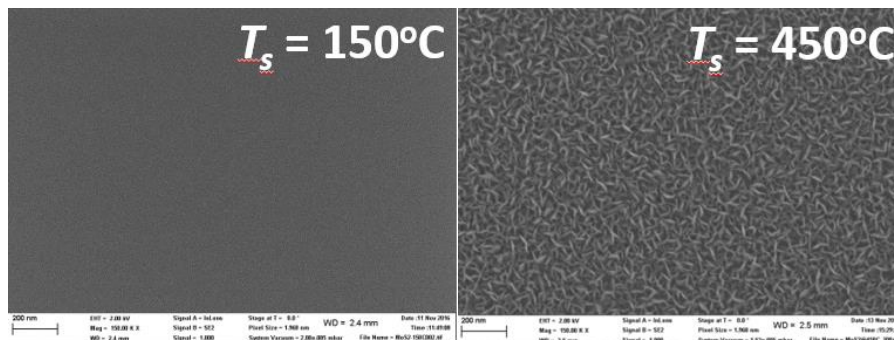

Figure 27: SEM images of synthesized MoS$_2$ for stage temperatures of 150 °C and 450 °C.

8. Results

Perovskite solar cells with a p-i-n structure were fabricated as shown in figure 28a. The *J/V*-characteristics for the perovskite solar cell with amorphous MoS_2, as well as the reference Cu:NiO-based solar cell, are shown in figure 28b. The figure clearly shows a lower V_{OC} and J_{SC} for the MoS_2-based PSC. This results also in a lower PCE value, although the fill factor (FF) is improved compared to the reference. The exact values are shown in figure 28c. This might signify a good band alignment between MoS_2 and the perovskite. Furthermore, the band structure of amorphous MoS_2 is still unknown. Another possible reason is that much recombination occurring within the perovskite layer leading to a loss of the V_{OC} and reduction in the J_{SC}. The main cause for the high recombination rate is probably the poor wettability of perovskite (hydrophobic) on MoS_2. The poor wettability may results in different perovskite crystal growth on the MoS_2 which increases the recombination rate and reduces the J_{SC}.

a)   b)   c)

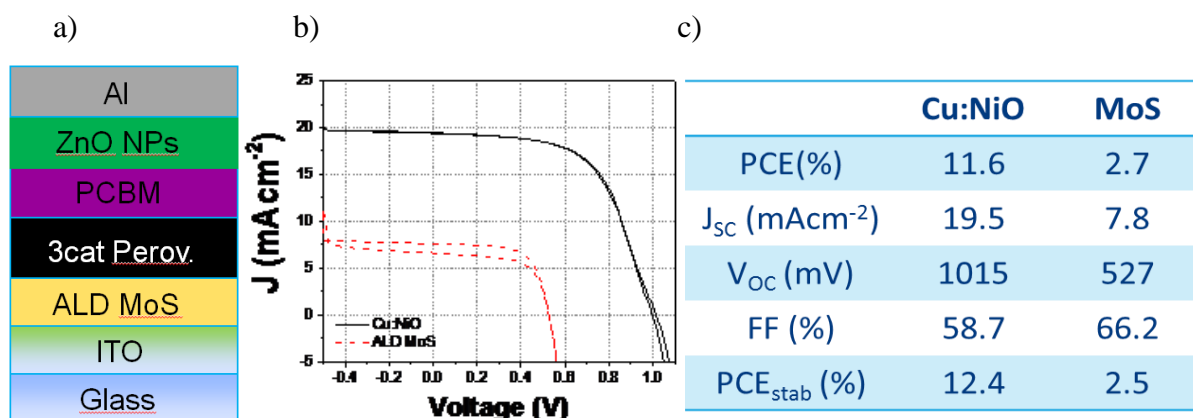|	Cu:NiO	MoS
PCE(%)	11.6	2.7
J_{SC} (mAcm^{-2})	19.5	7.8
V_{OC} (mV)	1015	527
FF (%)	58.7	66.2
PCE$_{stab}$ (%)	12.4	2.5

Figure 28: a) cell structure of the perovskite solar cell. b) J/V-characteristic for the PSC with MoS$_2$ and for the reference cell. c) Table with values

Another possible explanation for the low V_{OC} and J_{SC}, is that the MoS$_2$ layer absorbs a part of the incoming light. This is investigated by changing the thickness of the MoS$_2$ layer and measuring the PCEs. The PCEs for three different thicknesses (5, 10 and 15 nm) of MoS$_2$ are shown in figure 29. The figure shown no really differences in PCE for the different thicknesses. So from this measurements, it can be concluded that the MoS$_2$ doesn't operate as a light absorber, otherwise the PCE of the cell with 5 nm thick MoS$_2$ layer should be significantly higher than the PCE of the cell with 15 nm thick MoS$_2$.
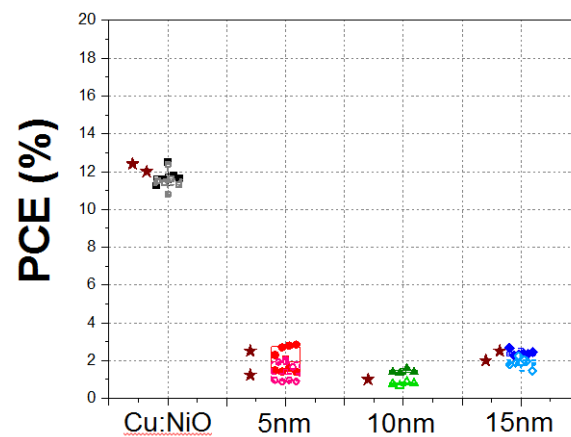

Figure 29: PCEs for different thicknesses of MoS$_2$ in the PSC.

9. Conclusion

The properties of MoS_2 show that it can be potentially used as a charge extraction layer in PSCs. Experiments employing ALD deposited amorphous MoS_2 as hole transport layer in Cs-containing triple cation PSCs are carried out. The MoS_2 films were synthesized by plasma enhanced ALD using alternating doses of molybdenum metal precursor and diluted H_2S plasma. The XRD, Raman and SEM images demonstrated the amorphous structure of the MoS_2 grown at stage temperature of 150 °C. Subsequently, the perovskite was deposited on the MoS_2 by spin coating. The fabricated perovskite solar cells yielded a good fill factor, however the performance was limited due to relatively low short-circuit current and low open-circuit voltage as compared to the reference. The low PCE of 2.7% was obtained, which could be due to several reasons. The primary reason identified is poor quality absorber (crystal growth) layer being deposited on MoS_2 as a result of poor wettability. This could lead to prominent recombination within the absorber bulk leading to a decrease in J_{SC} and V_{OC}. Additionally, the band gap of amorphous MoS_2 is still unknown, which can result in poor band alignment. The MoS_2 might also behave as an absorber of the light. However, by measuring the PCEs of the cells with different thicknesses of the MoS_2 layers is shown that the PCEs don't change for different thicknesses. This confirms that the predominant loss in J_{SC} is not duo to the parasitic absorption in the MoS_2 layer. Furthermore, some pathways are suggested that can improve the adhesion/wettability of the perovskite layer on MoS_2. Plasma pre-treatment of MoS_2 can result in a better wettability of the perovskite layer leading to better crystal growth. Also other literature already shown the potential of crystalline form of MoS_2. Several articles successfully implemented crystalline MoS_2 in PSCs, which resulted in better PCEs and improved stability of the cells. The literature overview and our results definitely show the good potential of MoS_2 for PSCs, but some more research has to be done improve the MoS_2-based PSCs.

Bibliography

[1] A. Kojima, K. Teshima, T. Shirai and T. Miyasaka, "Organometal halide perovskites as visible-light sensitizers for photovoltaic cells," *Journal of the american chemical society,* 2009.

[2] N.-G. Park, "Perovskite solar cells: an emerging photovoltaic technology," *Elsevier,* 2014.

[3] H.-W. Chen, T.-Y. Huang, T.-H. Chang, Y. Sanehira, C.-W. Kung, C.-W. Chu, M. Ikegami, T. Miyasaka and K.-C. Ho, "Efficiency enhancement of hybrik perovskite solar cells with MEH-PPV hole-transporting layers," *Nature,* 2016.

[4] Y. Yang and J. You, "Make perovskite solar cells stable," *Nature,* 2017.

[5] R. Sanders, "Major advance in solar cells made from cheap, easy-to-use perovskite," *UC Berkeley,* 2016.

[6] H.-R. Wenk and A. Bulakh, "Minerals: Their Constitution and Origin," Cambridge University Press, 2004.

[7] V. Zardetto, B. Williams, A. Perrotta, F. D. Giacomo, M. A. Verheijen, R. Andriessen and W. M. M. K. a. M. Creatore, "Atomic layer deposition for perovskite solar cells: research status, opportunities and challenges," 24 December 2016.

[8] M. A. Green and A. Ho-Baillie, "Perovskite solar cells: the birth of a new era in photoboltaics," *acs energy letters,* 2017.

[9] F. Toor, "Perovskite solar cell fever," *SPIE,* 2016.

[10] Z. Song, S. C. Watthage, A. B. Philips and M. J. Heben, "Pathways toward high-performance perovskite solar cells: review of recent advances in organo-metal halide perovskites for photovoltaic applications," *Photonics for Energy,* 2016.

[11] W. S. Yang, J. H. Noh, N. J. Jeon, Y. C. Kim, S. Ryu and J. Seo, "High-performance photovoltaic perovskite layers fabricated through intramolecular exchange," *Science,* 2015.

[12] G. Niu, X. Guo and L. Wang, "Review of recent progress in chemical stability of perovskite solar cells," 2015.

[13] T. Leijtens, G. Eperon, S. Pathak, A. Abate, M. Lee and H. Snaith, "Overcoming ultraviolet light instability of sensitized TiO2 with meso-superstructured organometal tri-halide perovskite solar cells," *Nature,* 2013.

[14] T. A. Berhe, W.-N. Su, C.-H. Chen, C.-J. Pan, J.-H. Cheng, H.-M. Chen, M.-C. Tsai, L.-Y. Chen, A. A. Dubaleb and B.-J. Hwang, "Organometal halide perovskite solar cells: degradation and stability," *Energy & Environmental Science,* 2016.

[15] X. Qin, Z. zhao, Y. Wang, J. Wu, Q. Jiang and J. You, "Recent progress in stability of perovskite solar cells," 2017.

[16] D. Wang, M. Wright, N. K. Elumalai and A. Uddin, "Stability of perovskite solar cells," *Elsevier,* 2016.

[17] A. Capasso, A. D. R. Castillo, L. Najafi, V. Pellegrini and F. Bonaccorso, "Spray deposition of exfoliated MoS2 flakes as hole transport layer in perovskite-based photovoltaics," Queensland University of Technology, 2015.

[18] A. Dashora, U. Ahuja and K. Venugopalan, "Electronic and optical properties of MoS2 (0 0 0 1) thin films: Feasibility for solar cells," 8 January 2013.

[19] M. A. Green and A. H.-B. a. H. J. Snaith, "The emergence of perovskite solar cells," 27 June 2014.

[20] A. Capasso, F. Matteocci, L. Najafi, M. Prato, J. Buha, L. Cina, V. Pellegrini, A. D. Carlo and F. Bonaccorso, "Few-layer MoS2 Flakes as Active Buffer Layer for Stable Perovskite Solar Cells," 2016.

[21] E. Singh, K. S. Kim and G. Y. Y. a. H. S. Nalwa, "Atomically Thin-Layered Molybdenum Disulfide (MoS2) for BulkHeterojunction Solar Cells," Stanford, 2017.

[22] H. Knoops, S. Potts, A. Bol and W. Kessels, "Atomic Layer Deposition," Department op Applied physics, Eindhoven University of Technology, Eindhoven, the Netherlands.

[23] B. A. Sperlinga, W. A. Kimes and J. E. M. a. P. M. Chu, "Time-resolved Fourier transform infrared spectroscopy of the gas phase during atomic layer deposition," May 2010.

[24] L. K. Tan, B. Liu, J. H. Teng, S. Guo and H. Y. L. a. K. P. Loh, "Atomic layer deposition of a MoS2 film," 3 July 2014.

[25] Y. G. Kim, K. C. Kwon, Q. V. Le, K. Hong, H. W. Jang and S. Y. Kim, "Atomically thin two-dimensional materials as hole extraction layers in organolead halide perovskite photovoltaic cells," 12 April 2016.

[26] V. Nicolosi, M. Chhowalla, M. S. S. Mercouri G. Kanatzidis and J. N. Coleman, "Liquid Exfoliation of Layered Materials," *Science,* 2013.

[27] P. Schulz, E. Edri, S. Kirmayer, G. Hodes, D. Cahen and A. Kahn, "Interface energetics in organo-metal halide perovskite-based photovoltaic cells," *Energy Environ. Sci.,* 2014.

[28] G. Divitini, S. Cacovick, F. Matteocci, L. Cina, A. D. Carlo and C. Ducati, "In sity observation of heat-induced degradation of perovskite solar cells," *Nature,* 2016.

[29] Y. Zhao and K. Zhu, "Organic-inorganic hybrid lead halide perovskites for optoelectronic and electronic applications," *Chem. Soc. Rev.,* pp. 655-689, 2016.

[30] P. Docampo, J. M. Ball, M. Darwich, G. E. Eperon and H. J. Snaith, "Efficient organometal trihalide perovskite planar-heterojunction solar cells on flexible polymer substrates," *Nature communications,* 2013.

[31] B. Peng, G. Yu, Y. Zhao, Q. Xu, G. Xing, X. Liu, D. Fu, B. Liu, J. R. S. Tan, W. Tang, H. Lu, J. Xie, L. Denk, T. C. Sum and K. P. Loh, "Achieving ultrafast hole transfer at the monolayer MoS2 and CH3NH3PbI3 perovskite interface by defect engineering," *acs nano,* 2016.